

Biomimetic evolutionary analysis: testing the adaptive value of vertebrate tail stiffness in autonomous swimming robots

J. H. Long, Jr.^{1,*}, T. J. Koob², K. Irving¹, K. Combie¹, V. Engel¹, N. Livingston³, A. Lammert⁴ and J. Schumacher⁵

¹Department of Biology, Program in Cognitive Science, and the Interdisciplinary Robotics Research Laboratory, Vassar College, Poughkeepsie, NY 12604, USA, ²Skeletal Biology, Shriners Hospital for Children, Tampa, FL 33612, USA, ³Department of Electrical Engineering and Computer Science, Case Western Reserve University, Cleveland, OH 44106, USA, ⁴Speech and Hearing Research, VA Medical Center and East Bay Institute for Research and Education, Martinez, CA 94553, USA and ⁵Department of Neurology, Columbia University, New York, NY 10032, USA

*Author for correspondence (e-mail: jolong@vassar.edu)

Accepted 21 September 2006

Summary

For early vertebrates, a long-standing hypothesis is that vertebrae evolved as a locomotor adaptation, stiffening the body axis and enhancing swimming performance. While supported by biomechanical data, this hypothesis has not been tested using an evolutionary approach. We did so by extending biomimetic evolutionary analysis (BEA), which builds physical simulations of extinct systems, to include use of autonomous robots as proxies of early vertebrates competing in a forage navigation task. Modeled after free-swimming larvae of sea squirts (Chordata, Urochordata), three robotic tadpoles ('Tadros'), each with a propulsive tail bearing a biomimetic notochord of variable spring stiffness, k (N m^{-1}), searched for, oriented to, and orbited in two dimensions around a light source. Within each of ten generations, we selected for increased swimming speed, U (m s^{-1}) and decreased time to the light source, t (s), average distance from the source, R (m) and wobble maneuvering, W (rad s^{-2}). In software simulation, we coded two quantitative trait loci (QTL) that determine k :

bending modulus, E (Nm^{-2}) and length, L (m). Both QTL were mutated during replication, independently assorted during meiosis and, as haploid gametes, entered into the gene pool in proportion to parental fitness. After random mating created three new diploid genotypes, we fabricated three new offspring tails. In the presence of both selection and chance events (mutation, genetic drift), the phenotypic means of this small population evolved. The classic hypothesis was supported in that k was positively correlated ($r^2=0.40$) with navigational prowess, NP , the dimensionless ratio of U to the product of R , t and W . However, the plausible adaptive scenario, even in this simplified system, is more complex, since the remaining variance in NP was correlated with the residuals of R and U taken with respect to k , suggesting that changes in k alone are insufficient to explain the evolution of NP .

Key words: vertebrae, axial skeleton, notochord, stiffness, swimming, navigation, robots, evolution.

Introduction

To test hypotheses about biomechanical adaptations, selection experiments on living populations offer the opportunity to analyze connections between genotype and phenotype (Garland, Jr, 2003), construct models that relate morphology, performance, and fitness (Arnold, 2003), and understand the separate impact of selection, chance and history (Travisano et al., 1995). Without living taxa, however, it is at best difficult to determine plausible mechanical functions from morphology alone (Alexander, 2003; Hutchinson and Gatesy, 2006; Lauder, 1995), let alone the adaptive value of a trait (Amundson and Lauder, 1994). Seeking a bridge between the morphology and fitness of extinct taxa, biologists have combined biomimetics and phylogenetics (Bels et al., 2003;

Kingsolver and Koehl, 1985), building biologically inspired physical or computer simulations to determine plausible performance changes associated with changes in morphology (Long, Jr et al., 2006a) or behavior (Long, Jr et al., 2006b). Inference from performance to fitness requires that the investigator also reconstruct a selection environment, an ecological situation in which to judge adaptive value (Brandon, 1990). Thus the goal is to understand how individuals and their environments might have plausibly interacted to produce the derived state from the ancestral. We call this approach biomimetic evolutionary analysis (BEA).

Inspired by evolutionary robotics (Nolfi and Floreano, 2000), we extend traditional BEA by adding fundamental evolutionary features: (1) genetics: quantitative trait loci (QTL)

coding biomimetic morphologies, (2) mutation and genetic drift: random processes creating variable offspring, (3) autonomous individuals: mobile robots competing against each other, (4) selection environment: a behavior-based environment and criteria judging the relative fitness of individuals, and (5) evolution *per se*: the population changing over generational time by selection, drift and mutation (Gillespie, 2004). Central to the explanatory power of this evolutionary approach are the random processes of drift and mutation. Without randomness, decisions about how to vary the phenotypes under selection are made by the investigator, leaving open the opportunity for unintentional bias to canalize evolutionary trajectories.

The morphology we analyze is the vertebrate axial skeleton, which has undergone at least four episodes of convergent evolution from the ancestral state of a continuous notochord to the derived state of a jointed vertebral column (Gardiner, 1983; Koob and Long, Jr, 2000). The classical interpretation (Goodrich, 1930) is that bony or calcified vertebral elements evolved to strengthen and stiffen the axis as an adaptation for more powerful swimming (Laerm, 1976; Laerm, 1979; Rockwell et al., 1938). The presence of vertebral centra, the elements that surround and constrict the notochord, is correlated with increased fast-start performance in osteichthyans (Lauder, 1980) and increased undulatory swimming speed in actinopterygians (Webb, 1982; Weihs and Webb, 1983). Conversely, species that possess an adult notochord, e.g. Atlantic hagfish *Myxine glutinosa*, white sturgeon *Acipenser transmontanus*, and shovelnose sturgeon *Scaphirhynchus platyrhynchus*, swim voluntarily at very slow speeds, less than one body-length per second in the laboratory (Long, Jr et al., 2002; Long, Jr, 1995; Adams et al., 1997). Correlations, however, hide the complex relationship between morphology and performance: sturgeon, even though they possess a notochord, can swim fast enough to breach (Sulak et al., 2002), and no single morphology alone determines burst swimming performance (Brainerd and Patek, 1998; Ghalambor et al., 2003).

To identify influential vertebral morphologies and relate them to a specific mechanical function, we focus on mechanical properties. For example, the addition of rigid artificial vertebrae to a hagfish's notochord increases its bending modulus, E (in Pa) (Long, Jr et al., 2004a). E combines with the second moment of area, I (in m^4), a cross-sectional shape factor, and length, L (in m) of a cantilevered beam (Summers and Long, Jr, 2006) to produce spring stiffness, k (in N m^{-1}):

$$k = 3EI / L^3. \quad (1)$$

Spring stiffness has been linked to swimming performance (Pabst, 1996). Experimental alterations to the body's k in swimming gar (Long, Jr et al., 1996), swimming whole-body preparations (Long, Jr et al., 1994) and swimming physical models (McHenry et al., 1995) has provided indirect evidence that k increases swimming speed by increasing tailbeat frequency, tailbeat amplitude or propulsive wavelength, respectively. Moreover, the axial skeleton provides 25% of the body's spring stiffness in pumpkinseed sunfish *Lepomis gibbosus*, and 70% in Atlantic hagfish *Myxine glutinosa*

(Summers and Long, Jr, 2006). These results support the classical hypothesis: vertebrae have an adaptive function in swimming, stiffening the axial skeleton, increasing swimming speed and, hence, enhancing swimming performance.

To test this adaptation hypothesis using BEA, we first created biomimetic notochords constructed of cross-linked gelatin, based on a process used to make artificial tendons (Koob and Hernandez, 2003). Varying among notochords are two QTLs, E and tail length L , which, given constant I , determine k (Eqn 1). We placed these phenotypically variable biomimetic notochords into propulsive tails and attached those constructs to three swimming robots. The robots, called 'Tadros', were modeled after the one-eyed, free-swimming tadpole larvae of ascidians (Urochordata, Phylum Chordata), which to our knowledge is the chordate swimmer with the simplest sensorimotor system (McHenry and Strother, 2003). Ascidian tadpole larvae navigate in three dimensions using helical klinotaxis, an algorithm that also works in two dimensions for surface-swimming robots (Long, Jr et al., 2003; Long, Jr et al., 2004b). Information from ascidians informs the reconstruction of the common ancestor of the urochordate-vertebrate clade, recently posited as a monophyletic taxon based on phylogenomic evidence (Delsuc et al., 2006). To assess the relative performance of the Tadros, we created a selection environment in which their performance was judged on their ability to forage: to swim quickly, smoothly and accurately to a food source and then to hold station in close proximity. In proportion to their fitness, the tails were allowed to reproduce in simulation, with mutation randomly varying the QTL for E and L , gametogenesis assorting the chromosomes, and mating, with its accompanying genetic drift, producing new offspring tails. Lack of a significant relation between k and NP would refute, in this system, the classical hypothesis.

Materials and methods

Since this work involves many steps, processes and experiments, we provide an overview of the BEA methodology (Fig. 1). Each element of the method is detailed in the sections that follow.

Biomimetic notochords and propulsive tails

Notochords were manufactured in a two-step process: (1) cylindrical hydrogels were fabricated from gelatin and (2) they were cross-linked with glutaraldehyde to achieve targeted values of E . All hydrogels were made of a 0.1 g l^{-1} concentration of powdered gelatin (porcine skin, Type A; Sigma, St Louis, MO, USA) dissolved in distilled water heated at temperatures below 100°C . Trapped air bubbles were allowed to escape before the liquid was poured into cylindrical molds of 1.0 cm inner diameter and cooled at 6°C . Once solidified, the hydrogels were carefully pushed out of the molds and were visually inspected for damage; those with tears, pits or other imperfections were discarded. Undamaged hydrogels were cut to the desired length.

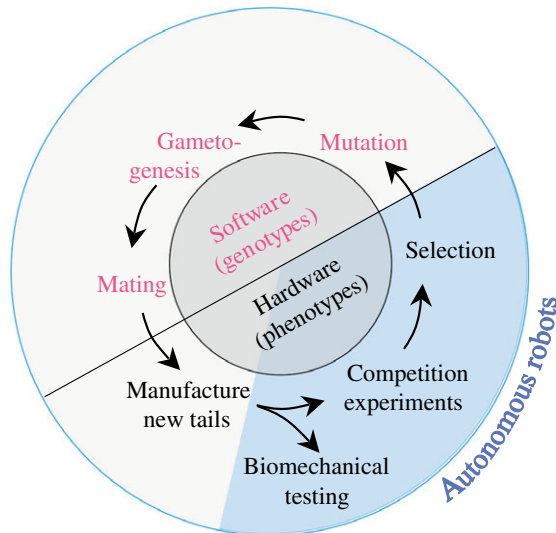


Fig. 1. Methodological approach to biomimetic evolutionary analysis using evolutionary robotics. In software (red font), a genetic algorithm is used to create randomly variable genotypes. In hardware (black font), those genotypic codes are used to manufacture biomimetic tail phenotypes that, in turn, are outfitted onto autonomous robots for biomechanical testing and competition experiments. The research cycle is repeated for ten generations.

To adjust the E values, hydrogels were cross-linked using various % concentrations of glutaraldehyde (25% EM grade; Polysciences, Warrington, PA, USA). The glutaraldehyde was diluted in phosphate buffer solution ($0.1 \text{ mol l}^{-1} \text{ NaH}_2\text{PO}_4$, $0.15 \text{ mol l}^{-1} \text{ NaCl}$, pH 7.0). Hydrogels bathed in the solution were placed on a shaker bed, left to cross-link for about 17 h, and then rinsed five times in distilled water to remove any remaining unreacted glutaraldehyde. Hydrogels were stored aseptically in an aqueous solution of 20% ethanol. To determine the relationship between concentration and E , we created a preliminary range of hydrogels cross-linked at various glutaraldehyde concentrations. The resulting hydrogels were bent at 1 Hz in three-point bending (Mini Bionix 858 with 10 N load cell; MTS Systems, Eden Prairie, MN, USA), resulting in the following equation:

$$E = 0.1159[\text{glut}\%] + 0.2017, \quad (2)$$

where E is in units of MPa.

After producing ten generations of biomimetic notochords using the formula (Eqn 2) for evolutionary trials, we validated the hydrogels' targeted E values in a custom-built cantilevered bending machine (Long, Jr et al., 2006a) that mimicked the cantilevered bending of the hydrogel mounted in the robots during swimming. We bent biomimetic notochords at a frequency of 1.76 Hz, near the operating tailbeat frequency of 1.70 Hz during swimming (Table 1), at flexions of 0.287 rad, near the operating tail flexion of 0.267 (see Table 3). All 30 evolved tails were tested in random order; two tails were randomly chosen and were retested three times throughout the procedure to measure repeatability, one minus the ratio of the

Table 1. Morphologic features and operating parameters of the Tadros

Feature or parameter	Mean \pm s.d.
Hull displacement (ml)	866 \pm 7.6
Tail displacement (ml)	19.0 \pm 5.2
Hull mass (g)	841 \pm 0.1
Tail mass (g)	15.5 \pm 0.1
Hull radius (m)	0.085 \pm 0.0001
Hull draft without keel (m)	0.051 \pm 0.001
Keel depth (m)	0.050 \pm 0.002
Tailbeat frequency f (Hz)	1.70 \pm 0.016
Lateral amplitude of tail tip a (m)	0.009 \pm 0.0003
Tail-length-specific tailbeat amplitude	0.141 \pm 0.0057
Froude number η	0.226 \pm 0.0054
Reynolds number at 20°C	11 730 \pm 237

All measurements of morphologic features are from 3–5 replicates.

Tail displacement and mass are examples from a single tail (generation 7, intermediate k).

Operating parameters are means ($N=30$) from biomechanical tests (see Table 3).

Hull diameter of 0.170 m was used as the characteristic length for Reynolds number.

measurements' standard deviation (s.d.) and mean value. We had an average repeatability of 93% and the 30 E values did not differ significantly (two-tailed paired t -test, $P=0.137$) from the targeted E values from Eqn 2. These were the E values we used.

The biomimetic notochords were used as the axial skeleton in the propulsive tail (Fig. 2). The ends of the notochords were gripped with heat-shrink tubing that was, in turn, glued on one end to an insert screwed into the driveshaft and on the other end to a rigid and flat hemi-circular tail of acrylic (Fig. 2). To prevent the tail from sagging or lifting in the vertical plane, a vertical septum was created from two conjoined sheets of Press and Seal™ wrap (Glad, Oakland, CA, USA); the septum cradled the notochord and secured the caudal fin to the driveshaft. While the depth of the driveshaft side of the vertical septum was held constant, the axial length of the vertical septum co-varied with the length of the tail. Finally, in lateral bending tests, we were unable to detect the presence of the vertical septum, since its contribution to stiffness was within the margin of repeatability (see above).

Biomimetic robotic tadpoles: Tadros

The Tadros is an autonomous, self-propelled agent, capable, using a single photoresistor 'eye', of detecting a light gradient, swimming up the gradient, and orbiting around the spot of greatest light intensity (Long, Jr et al., 2003; Long, Jr et al., 2004b). For surface swimming, we call this behavior two-dimensional, cycloptic helical klinotaxis (2D cHK). We modified the previous 2D cHK Tadros design by replacing the analog circuit implementation of the neural algorithm with a digital microcontroller (MIT HandyBoard, Newton Labs, Renton, WA, USA). The microcontroller allows us to use a

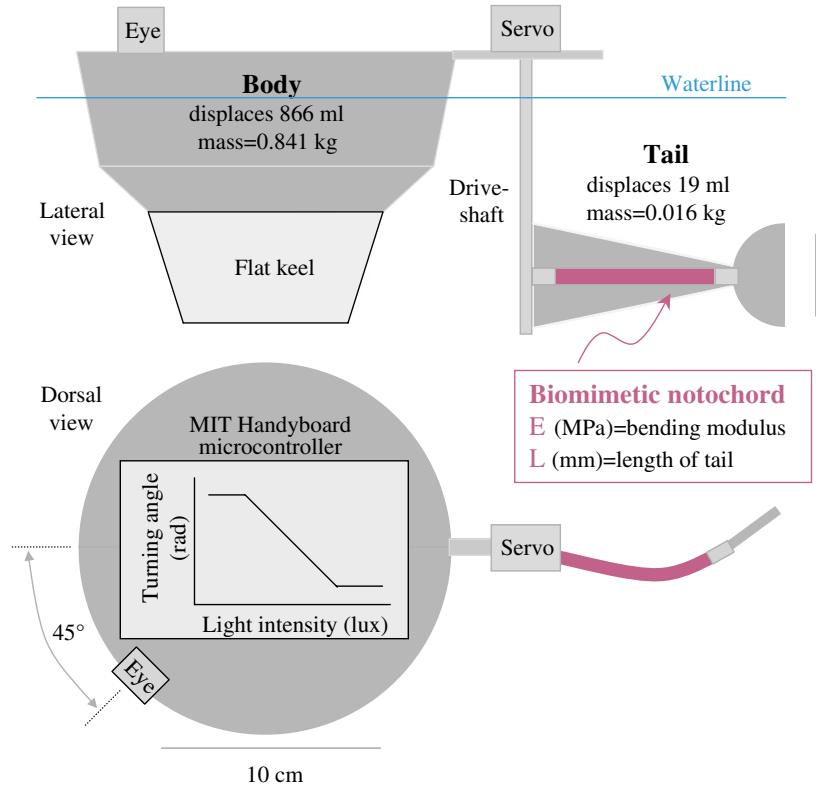


Fig. 2. Biomimetic tadpole robot ('Tadro') with biomimetic tail. Modeled after the free-swimming larvae of the sea squirts (subphylum Urochordata), the robots have a single eyespot (photoresistor), a flapping tail, and a microcontroller that converts the light intensity at the eyespot into a turning angle at the tail. This sensorimotor system produces autonomous phototactic navigation (Long, Jr et al., 2004b). New to this version of the Tadros are the digital microcontroller, servo tail flapper, and the biomimetic gelatin hydrogel of the tail serving as a notochord. The notochord's spring stiffness, k , is determined by bending modulus E and length L , which are coded as quantitative trait loci. The flapping amplitude of the servo motor was constant at $\pm 30^\circ$. The tail position had a range of 180° . See Table 1 for additional operating and morphological parameters.

single servomotor (MPI MX-400, Maxx Products, Lake Zurich, IL, USA) to both flap and turn the tail (Fig. 2). Controlled by software (Interactive C, v. 4; Newton Labs; working code available from J.H.L. upon request), the servomotor flapped the tail $\pm 30^\circ$ at a nearly constant cycle frequency of 1.7 Hz producing lateral tail-tip amplitudes that operated the tail at Froude numbers of 0.226 (Table 1), within the range seen in fish and close to but not within the lower limit considered optimal for thrust production (Terada and Yamamoto, 2004; Triantafyllou et al., 1993). The Tadros operate at Reynolds numbers near 11 730 (Table 1). Voltage across the single cadmium sulphide (CdS) photoresistor 'eye' (Fig. 2) varied inversely with light intensity and was converted to a tail offset that varied continuously and independently from the sinusoidal flapping.

Competition experiments with forage navigation

In each generation, we tested three tails, each bearing a biomimetic notochord with a different value of spring stiffness, k . We limited the population size to three so that we could compete three Tadros simultaneously, allowing their physical interactions to be part of the selection environment (Fig. 3A). While we built three Tadros of identical specifications and parts, we did not assume that they would perform identically. To control for differences among the Tadros, independent of those caused by the different tails, we ran 12 competition experiments in each generation, with all six possible combinations of tails and robots replicated twice.

Each trial was 3 min long, and began with Tadros directed

towards the center of a 2.5 m diameter circular tank (Fig. 3B). Starting position was randomized for all twelve trials. A light source was suspended above the tank, creating on the water surface an area of high intensity (Fig. 4A) and a rapidly attenuating gradient (Fig. 4B). We measured the Tadros' ability to perceive the light gradient, and confirmed that their perception varied with both distance from and orientation to the light source (Fig. 4C).

The three Tadros were videotaped from above (JVC digital video; 30 Hz temporal resolution; 1.2 cm spatial resolution), under light provided only by the target light source. To mark the bow, stern and identity of each Tadro, they carried colored LEDs. Digital videos were converted to QuickTime movies and analyzed using VideoPoint (ver. 2.5, Lenox Softworks, Lenox, MA, USA). Bow and stern points on each of the three Tadros were manually digitized every 1 s, for a total of 120 frames and 720 points per trial.

For our behavioral metric, we recognized the coordination required between functional systems to enact behavior (Rice and Westneat, 2005). The navigational task was to move towards the light source, find it quickly, and hold station in a tight orbit around that source. This involves possible trade-offs: swim quickly to get to the target but then maneuver to stay as close to the target as possible. An idealized agent would swim quickly to the source and then stop, moving only as needed to stay on the target. For our simple swimmers, however, they are behaviorally constrained because they are constantly swimming; the only motor output controlled by the brain is turning direction. Since forage navigation involves detection,

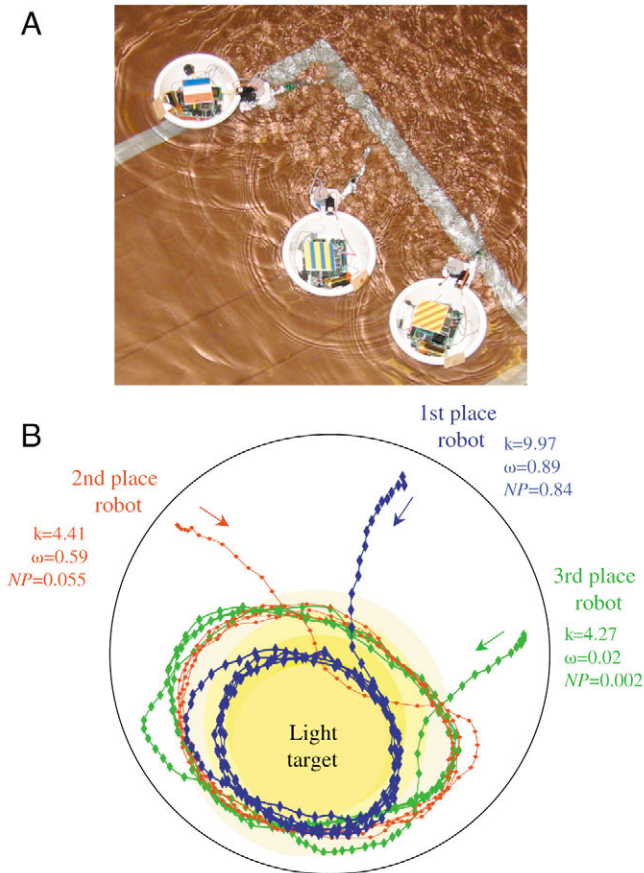


Fig. 3. Biomimetic Tadros compete in phototactic forage navigation. (A) Three prototype Tadros swim during the initial light-detection phase. Note that Tadros interact physically and compete within a generation; thus they are an evolving part of the otherwise stable selective environment. (B) Trajectories of three Tadros in one trial (generation 1, trial 4 of 12), showing the differences in orbital radius around the light target. Fitness ω rewards a small orbital radius R , short time to find the target t , fast swimming speed U and low robot wobble W . Here tail stiffness k is correlated with fitness ω and navigational prowess NP .

propulsion, maneuvering, and station-holding, we created ‘navigational prowess,’ NP , a dimensionless number:

$$NP = U / RtW, \quad (3)$$

where U (m s^{-1}) was the average forward speed of propulsion, taken as the finite difference in midpoint position of the Tadro’s hull along its trajectory over each 1 s time increment (0.01 m s^{-1} resolution). R (m) was the orbital radius, the average distance of the Tadro from the light target (Fig. 3) and a measure of station-holding ability. t (s) was the time to the food source, which was defined as within 0.5 m of the spot of highest intensity (Fig. 3); Tadros that failed to get this close received the maximum time of 120 s. W (rad s^{-2}) was the yaw wobble of the Tadro, defined as the s.d. of the Tadro’s angular acceleration in yaw (rad s^{-2}), as determined by finite differences of the angular velocity (rad s^{-1}), which was also determined from finite differences of the heading (rad) between

frames. W measures both recoil caused by periodic tail beats and accelerations caused by turning maneuvers (Fig. 5), and was developed as a proxy of path tortuosity, a key parameter in animal orientation and searching that is inversely related to the efficiency of the orientation mechanism (Benhamou, 2004). Taken together in NP , these kinematic variables define more effective forage navigation, which we defined as higher values of NP . Higher values of NP can be generated in a variety of ways given the number of variables. Thus the complexity of NP as a behavioral metric permits the evolution of different phenotypes that produce equivalent performance.

Individual fitness, ω_i , is the chance of survival of the genotype (Ridley, 1993), a number between 0 and 1. The ‘individual’ here, denoted by the subscript i , was one of three tails each generation. The individual relative fitness, ω_{ij} , relative to that of other individuals in the particular generation, where generation was indicated by the subscript j , was computed, following 12 experimental runs per generation, as follows:

$$\omega_{ij} = \frac{1}{4} \left[\left(\frac{R_{j\max} - R_{ij}}{R_{j\max} - R_{j\min}} \right) + \left(\frac{t_{j\max} - t_{ij}}{t_{j\max} - t_{j\min}} \right) + \left(\frac{U_{ij} - U_{j\min}}{U_{j\max} - U_{j\min}} \right) + \left(\frac{W_{j\max} - W_{ij}}{W_{j\max} - W_{j\min}} \right) \right], \quad (4)$$

where the j_{\max} and j_{\min} terms were the maximum and minimum values, respectively, for all individuals performing in that generation, j . Without *a priori* biological knowledge about the relative importance of each, we weighted the kinematic phenotypes equally.

Biomechanical analysis

In biomechanical analyses, we sought more detail about the motion of the tails during swimming. Each Tadro was filmed separately from below as they swam straight in a clear Plexiglas™ tank (JVC digital video; 30 Hz temporal resolution; 0.25 cm spatial resolution). Two points on the hull were tracked (bow and stern) in addition to three points on the notochord, one on either end and one in the middle. All five points were manually digitized as above every 1/30 s for three tailbeat cycles. Each of the 30 tails was tested three times, once on each of the three Tadros, for a total sample size of 90.

In addition to calculating swimming speed U and wobble W , as above, we used the positional data on the notochord to calculate tailbeat frequency f (Hz), tail flexion ϕ (rad), lateral amplitude of the tail tip a (m), phase of lateral tail displacement δ (% cycle), and Froude number η (non-dimensional). Tailbeat frequency f was measured as the inverse of the average period (s) of the beating tail over three tailbeats (resolution of 30 Hz). Tail flexion ϕ was measured as the angular deviation of the three points on the tail from a straight line (resolution of 0.009 rad). Lateral amplitude of the tail tip a was measured as half of the average maximal difference between positions of the tail (resolution of 0.001 m). Phase of lateral tail displacement δ was measured as the difference in time between

the attainment of maximal lateral position of the middle and distal points on the tail (resolution of 5 % of cycle). Froude number η was calculated as the ratio of the product of f and a to U .

Genetic algorithm

Genetic algorithms were used to simulate the interaction of mutation, genetic drift, mating and selection in artificial evolution (Nolfi and Floreano, 2000). Genotype frequencies after selection, p'_{ij} , were computed as follows:

$$p'_{ij} = p_{ij}\omega_{ij}, \tag{5}$$

where p_{ij} was the genotype frequency prior to selection, which, before we applied selection, was equal for all three genotypes with $p_{ij}=0.333$. After selection, the frequencies were as follows:

$$p'_{ij} = 0.333\omega_{ij}. \tag{6}$$

Since the sum of the all the genotype frequencies no longer equaled one, we calculated the normalized genotype frequency, p''_{ij} , which was used to determine the number of gametes that each parent contributes to the gene pool:

$$p''_{ij} = \frac{p'_{ij}}{\omega_j}, \tag{7}$$

where $\bar{\omega}_j$ was the mean relative fitness (Ridley, 1993) of the population at generation j :

$$\bar{\omega}_j = \sum \frac{\omega_{ij}}{3}. \tag{8}$$

Gametogenesis and mating

Prior to mating, each parent genotype underwent simulated gametogenesis *via* meiosis with mutation but no recombination. For each QTL, we assumed simple additive genetic variance without dominance or epistasis. The diploid adult genotype $(E_1/E_2, L_3/L_4)_{ij}$ consisted of two QTLs, E and L (where the trait denotation is a capital letter italicized and the chromosome letter is not) with a large but unspecified finite number of loci, with loci for each trait located on separate chromosomes as indexed by the subscripts. Given an isomorphic relation between genotype and phenotype (narrow-sense heritability of one), we represented genotype quantitatively using the continuous values for the adult phenotype. For simplicity, we partitioned the quantitative phenotype equally between the two sister chromosomes.

During meiosis, we mutated each of the four chromosomes, E_1, E_2, L_3, L_4 , of each individual. The magnitude and sign of mutational change was determined by randomly selecting a value from a Poisson distribution, where the center of the distribution was zero change and the range was scaled to encompass $\pm 25\%$ of the trait's median value. (For E , range and median were 0.1 to 1.4 MPa and 0.65 MPa, respectively; for L , range and median were 20 to 120 mm and 70 mm, respectively.) Mutation created four new chromosomes for each individual, $E_1^*, E_2^*, L_3^*, L_4^*$, and 12 new chromosomes for

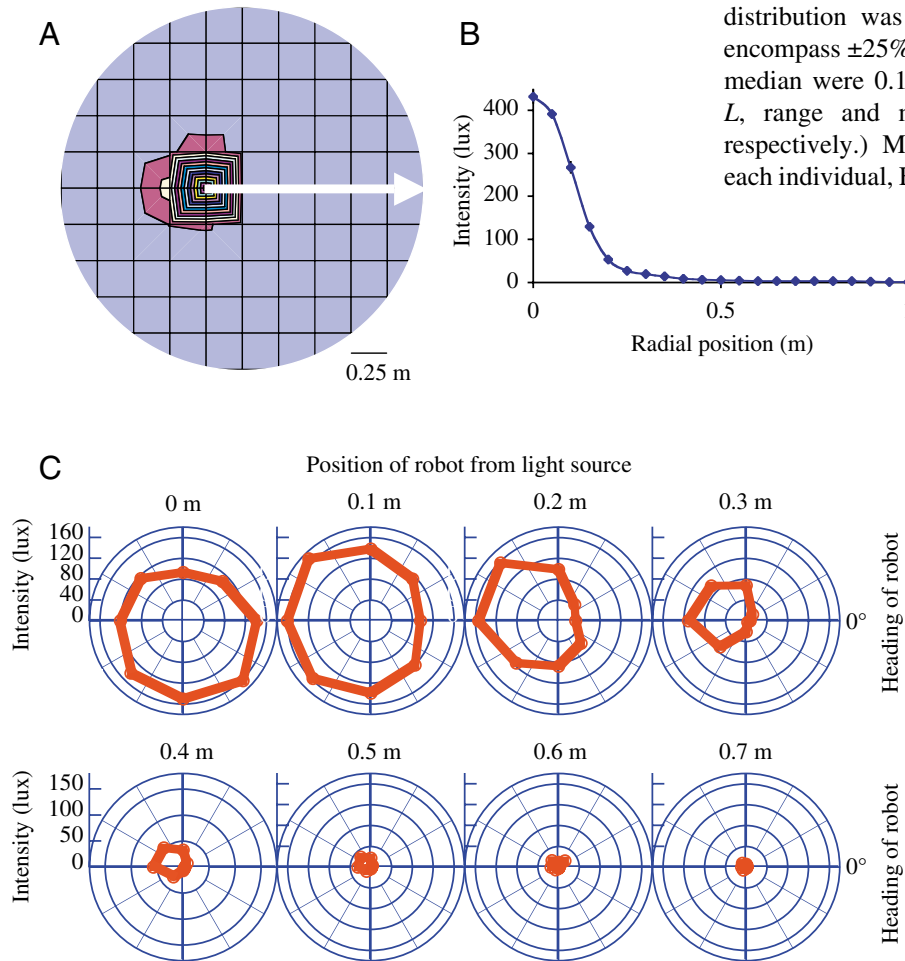


Fig. 4. Light and perceptual environments for Tadros. (A) Overhead view of light environment in experimental tank, with color gradient showing position of light source. Arrow indicates radial slice shown in B. (B) Light intensity gradient along radial indicated in A. (C) Perception of light gradient by Tadros. Polar plots indicate light intensity (along radii, with origin at 0 lux) registered by Tadros at different headings every 0.1 m along radial slice shown in B. A heading of 0° means that the Tadros was facing in the direction indicated by the arrow in A. Note eyespot is located 45° to the left of the Tadros's centerline (see Fig. 2).

the population. By segregation and independent assortment, each of the three individuals creates, four gamete types with the following haploid genotypes:

$$(E_{1*}, L_{3*})_{ij+1}, (E_{1*}, L_{4*})_{ij+1}, (E_{2*}, L_{3*})_{ij+1}, (E_{2*}, L_{4*})_{ij+1} .$$

For mating, six gametes were chosen for the gene pool. Each individual contributed to the pool on the basis of their post-selection normalized genotype frequency, p_{ij}^g (Eqn 7), which determined their number of gametes, N_{ij} :

$$N_{ij} = 6p_{ij}^g . \quad (9)$$

Thus, for an individual, N_{ij} gametes were chosen randomly from the four possible types. The combined gene pool of six gametes was then randomly combined in pairs to create the new generation of three diploid individuals.

Because of the small population size of three, selection results in differential reproduction, and hence evolution by selection, only if the differences among individual fitnesses results in a value of p^g greater than 0.5 for one individual. When all values of p^g are below 0.5, each individual contributes two gametes and evolution by selection is therefore not present. This is the

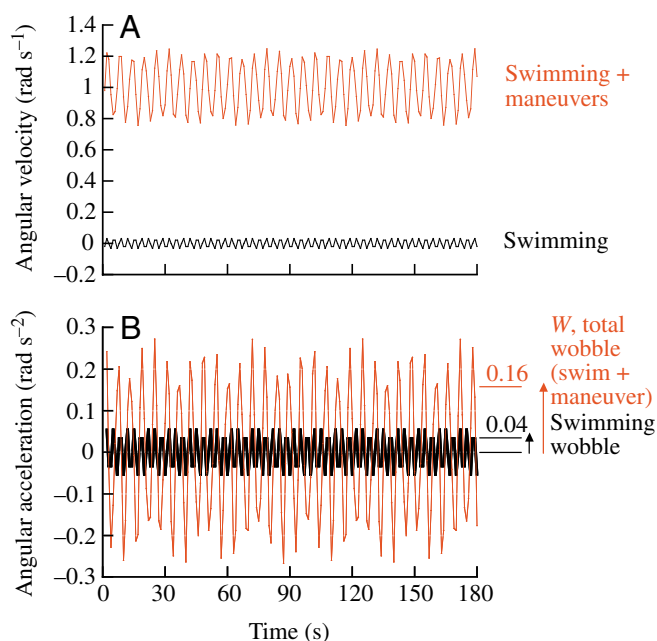


Fig. 5. Wobble W measures unsteady turning maneuvers. Defined as the standard deviation of the angular acceleration experienced by the Tadro's hull, W includes acceleration from the yaw recoil of swimming and the turning maneuvers exercised by the Tadro as it seeks light and maintains station about the light source. (A) This hypothetical situation shows how angular velocity added to swimming yaw (dark line) yields the total angular velocity (red) line, the difference being the maneuvering velocity added to swimming. (B) Angular acceleration of the data from the hypothetical situation shows how W measures its dispersion about the mean value. Simple sinusoidal model of angular velocity with realistic values for tailbeat frequency (1.7 Hz) and W chosen as parameters (see Results). The value for unsteady turning maneuvers (0.17 Hz) was estimated from trials.

distinction we use with the phrases 'with selection' and 'without selection', respectively. Please note that always present is evolution by chance, which includes mutation and drift.

Statistical design

To normalize the response variables from the competition trials, a variety of transforms were run, and the best, as judged by the linearity of probability plots, were used (Zar, 1996). E was normally distributed and untransformed; L and k were \log_{10} -transformed. R , U , W and NP were arcsine-square-root transformed, with R first divided by 10; t was inverse transformed. For the biomechanical analysis, data were \log_{10} -transformed. All statistics were performed using JMP (ver. 5.0, SAS Institute).

The competition trials were analyzed in four ways. First, to determine if evolution had occurred, we conducted a nested ANCOVA with generation as the main effect, Tadro as the covariate, and tail nested within generation ($N=360$; for each of 10 generations, three tails tested in 12 trials). This model was used on the response variables, R , t , U , W and NP , with planned *a priori* contrasts ($\alpha=0.05$) to examine generation-to-generation changes in the population mean. Second, to address the same question for the morphological phenotypes, E , L and the mechanical behavior, k , we simplified the model to a one-way ANOVA, with generation as the effect ($N=30$), which included planned *a priori* contrasts ($\alpha=0.05$) to examine generation-to-generation changes in the population mean. Third, to determine if evolutionary changes in the population mean differed when the population was under selection and when it was not, we created new response variables, for example ΔE , that took the difference in the population mean from generation j to $j+1$. Since there are nine intergenerational intervals, this yielded a sample size for each new response variable of nine. We ran a one-way ANOVA with selection (absent, present) as the effect. Fourth, to examine the correlation structure between k and NP , as mediated by the kinematic variables, R , t , U and W , we ran a one-way MANOVA ($N=30$), which yielded partial correlation coefficients and univariate regressions of the responses onto k . Using those regressions, we generated predicted values of R , t , U and W and compared those to the observed; residuals were calculated as the difference between observed and predicted values. The residuals of R , t , U and W were used as a set of possible predictor variables for the residuals of NP , and step-wise linear regressions (forward, backward, mixed models) were run.

The biomechanical analysis of k and swimming kinematics

Table 2. Morphologic and mechanical properties of the 30 evolved tails

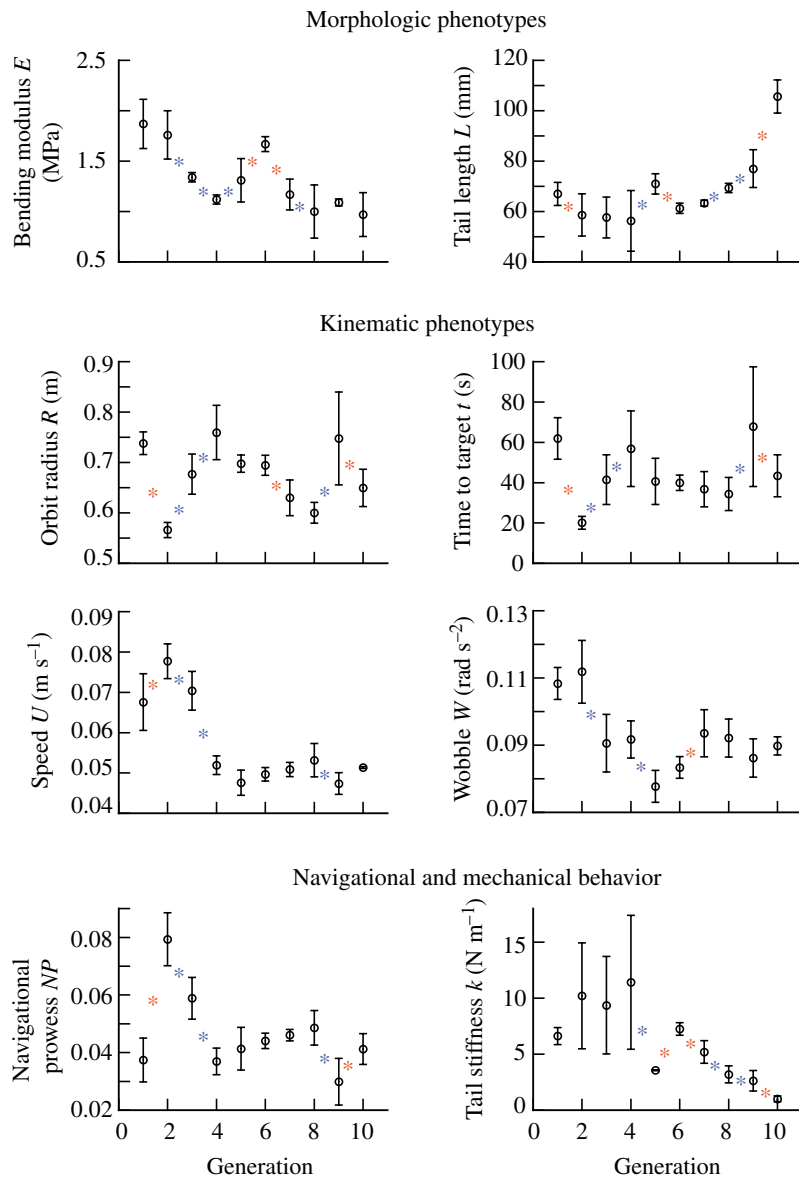
	Mean \pm s.d.	Range
Bending modulus E (MPa)	1.329 \pm 0.4049	0.495–2.318
Tail length L (m)	0.069 \pm 0.0169	0.038–0.115
Second moment of area I ($\times 10^{-10}$ m ⁴)	3.48 \pm 0.405	2.69–4.53
Tail stiffness k (N m ⁻¹)	6.049 \pm 5.3065	0.564–22.735

Table 3. Kinematic properties of the Tadros and tails during rectilinear swimming

	Mean \pm s.d.
Swimming speed U (m s^{-1})	0.069 \pm 0.0014
Wobble W (rad s^{-2})	0.040 \pm 0.0016
Tailbeat frequency f (Hz)	1.70 \pm 0.016
Lateral amplitude of the tail tip a (m)	0.009 \pm 0.0003
Tail flexion ϕ (rad)	0.267 \pm 0.0049
Phase of lateral tail displacement δ (% cycle)	18.3 \pm 1.02
Froude number η	0.226 \pm 0.0054

For this biomechanical analysis $N=30$.

(a , f , U , W , δ , ϕ and η , recorded in straight-swimming trials) was conducted using linear regression ($N=30$, from the mean of three trials for each of 30 tails).



Results

The thirty tails evolved over ten generations had variable morphological and mechanical properties (Table 2). In non-navigational rectilinear swimming during the biomechanical analysis, the Tadros and tails also had variable kinematics (Table 3). Unexpectedly, we encountered two uncontrolled sources of variation in the fabrication of the notochords and the Tadros. First, the notochords' second moment of area, I (m^4), which was meant to be held constant (see Materials and methods), instead varied in inverse proportion to E (MPa):

$$I = -6.12 \times 10^{-11} E + 4.29 \times 10^{-10}, \quad (10)$$

with a coefficient of determination of 0.375 ($N=30$; $P<0.001$). Because of this covariation, calculations of k for each tail used an actual I and not an I assumed from the fabrication process. Second, even though the three Tadros were designed to be identical, they performed differently, as revealed by ANCOVA from the competition experiments. Treated as the covariate, the Tadro effect was highly significant ($P<0.001$) for R , U and W . This result justified our experimental design, where each tail was tested 12 times per generation, four times on each of the three Tadros.

The Tadros showed variation in navigational behavior that was sometimes, but not always, correlated with phenotypic variation in k (Fig. 3). Over ten generations, the population mean of NP and k evolved, changing significantly in five and six generational intervals, respectively (Fig. 6). Evolution occurred in all other phenotypes as well. With every phenotype, the direction of evolution varied. Moreover, evolution of at least three of the eight phenotypes occurred in every inter-generational time step (Fig. 6).

In the presence of selection in generations 1, 5, 6 and 9, unidirectional evolution of the population mean, relative to that when selection is absent, occurred in five of the eight phenotypes (Fig. 7). The morphological phenotypes, E and L , showed no significant unidirectional trend; likewise for k , although the non-significant trend was for k to increase in the presence of selection. The behavioral phenotype NP increased in the presence of selection; this was not surprising,

Fig. 6. Evolution of morphology and behavior of the robotic population. Significant changes in population means between generations are indicated with an asterisk midway between the points ($\alpha=0.05$; planned *a priori* contrasts in nested ANCOVA on data transformed to create normal distribution, with $\log L$, k ; arcsine R , U , W , NP ; inverse t). Red asterisks indicate changes driven by selection and chance (drift + mutation); blue asterisks chance only. Selection occurred in generations 1, 5, 6 and 9. Values are means \pm s.e.m.

since NP is a composite of the kinematic phenotypes R , t , U and W , all of which changed unidirectionally in the presence of selection (Fig. 7). Note that the directions of change differ: R and t increased while U and W decreased in the presence of selection. Thus the increases in W correlated with the increases in U counteract (Eqn 3).

From the biomechanical analysis and competition trials, k predicted U of the biomimetic robots (Fig. 8A). The only other kinematic phenotype that was measured in both the biomechanical analysis and the competition trials, W , was predicted by k only in the competition trials (Fig. 8B). Since W

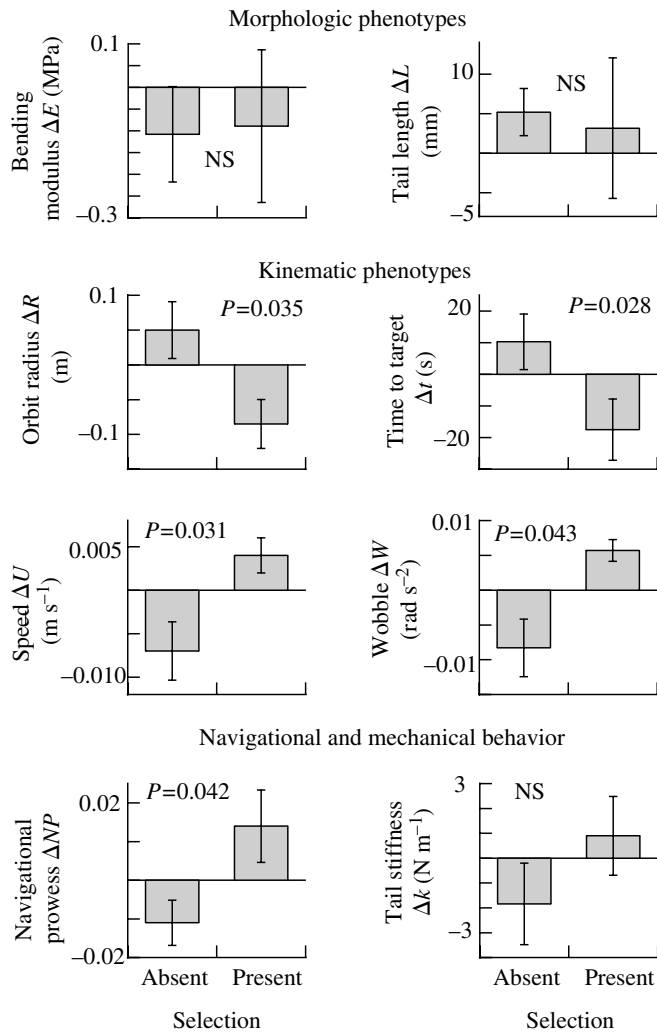


Fig. 7. Unidirectional evolution in response to selection. Evolutionary change measured as the difference in population means between generations, Δx , with changes grouped by absence ($N=5$) and presence ($N=4$) of selection. Selection occurred in generations 1, 5, 6 and 9; chance occurs throughout. Neither of the genetically based traits, E and L , evolved unidirectionally in response to selection. The four components of fitness, R , t , U and W , evolved unidirectionally in response to selection. Navigational prowess increases in response to selection, while tail stiffness k does not. Significance determined using one-way ANOVA on data transformed to create normal distributions ($\log L$, k ; arcsine R , U , W , NP ; inverse t). Values are means \pm s.e.m.

includes angular acceleration from both yaw recoil of the flapping tail during rectilinear swimming and unsteady turning maneuvers (see Fig. 5), the difference between competition and biomechanics trials was a measure of the portion of the W caused by unsteady maneuvering. Thus k was unrelated to the rectilinear swimming W (biomechanical analysis) and was positively correlated with greater unsteadiness during maneuvers, W (competition trials). For the competition experiments, the kinematic phenotypes were correlated, with negative correlations between R and U , R and $1/t$, R and W , and positive correlations between U and $1/t$, U and W (Table 4). Note that these correlations were performed on transformed data and that the sign of the correlations with $1/t$ will be opposite those with t .

From the biomechanical trials alone, k predicted only a (Fig. 9A), which, in turn, significantly predicted U (Fig. 9B). All other biomechanical response variables (f , δ , ϕ and τ) are not predicted by k in linear regression.

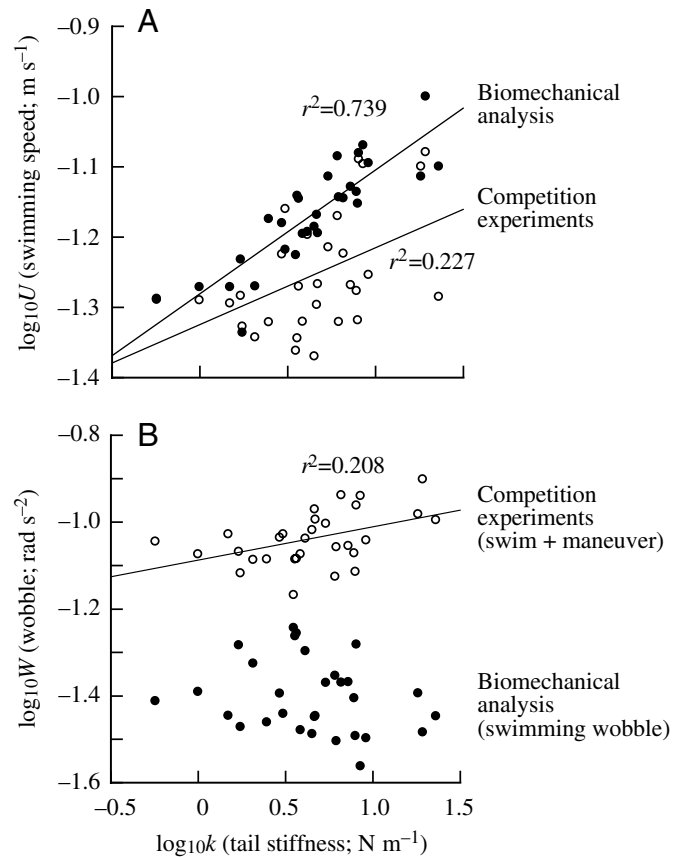


Fig. 8. Tail stiffness k predicts the kinematic phenotypes (A) swimming speed U and (B) robot wobble W . Data for competition experiments (open circles) are means of 12 navigation trials for each of 30 tails. Data for biomechanical analysis (closed circles) are means of three straight-swimming trials for each of 30 tails. Lines indicate significant ($\alpha < 0.01$) regressions on log-transformed data; data without a line failed the significance test at $\alpha < 0.05$. Note that W for the competition experiments includes wobble caused by swimming and maneuvering (see Fig. 5).

Table 4. Correlations of kinematic phenotypes during competition experiments

	arcsine $R/10$	$1/t$	arcsine U	arcsine W
arcsine $R/10$	–	–0.612*	–0.480*	–0.030
$1/t$	–0.868	–	0.370*	0.014
arcsine U	–0.517	0.562	–	0.360*
arcsine W	–0.206	0.279	0.545	–
$\log_{10}k$ slopes	0.0074	0.0067	0.0323*	0.0293*
$\log_{10}k$ intercepts	0.2567	0.0387	0.2177	0.2885

Above the diagonal, Pearson correlation coefficients with probabilities as follows: * $P < 0.01$. Sample size=360 (10 generations, 12 trials each generation, 3 Tadros each trial).

Below the diagonal, partial correlation coefficients from MANOVA with \log_{10} of spring stiffness k as the independent variable (sum response with orthogonalized responses; overall model and k significant, $P < 0.001$). Sample size=30 (10 generations, 3 tails each).

Bottom two rows hold the slope and intercept estimates from the univariate least-squares regressions for $\log_{10}k$ as independent variable to the kinematic variables.

All statistics run on data transformed to improve normality.

Note that the sign of correlations with t would be opposite that relative to same with $1/t$.

The trajectory of the population through $[E, L]$ morphospace was erratic (Fig. 10), as expected if both chance (drift and mutation) and selection were operating. Unexpected by the classical prediction of the benefit of increased k on navigational performance, however, was that when selection was present sometimes k increased (steps 1–2 and 5–6) and sometimes it decreased (6–7 and 9–10). Changes in the \log_{10} of k , mediated through the kinematic variables (Eqn 3; Table 4), predicted 40% of the variation in NP (Fig. 11A). Of the variance in NP unexplained by k , measured as the NP residuals, 81% was inversely and positively correlated with the residuals in R and U , with slopes of -0.115 and 0.610 , respectively (Fig. 11B). The trajectory of the population through $[NP, k]$ behavior space appeared erratic, but a pattern emerged (Fig. 12). Whenever selection was present, NP increased, independent of changes in k . At this landscape level, the evolutionary histories of k and NP appeared decoupled, in spite of the linkage between the two seen by the significant relation between k and U (Fig. 6A), k and W (Fig. 8B), and k and NP (Fig. 11A). When taken in sum, the functional relation between k and NP was complex enough (Fig. 13) to permit multiple evolutionary outcomes.

Discussion

This is the first study, to our knowledge, that evolves autonomous biomimetic robots to test an adaptation hypothesis for vertebrates. This extension of biomimetic evolutionary analysis (BEA) permits the functional relation between morphology, mechanics, and behavior to be varied

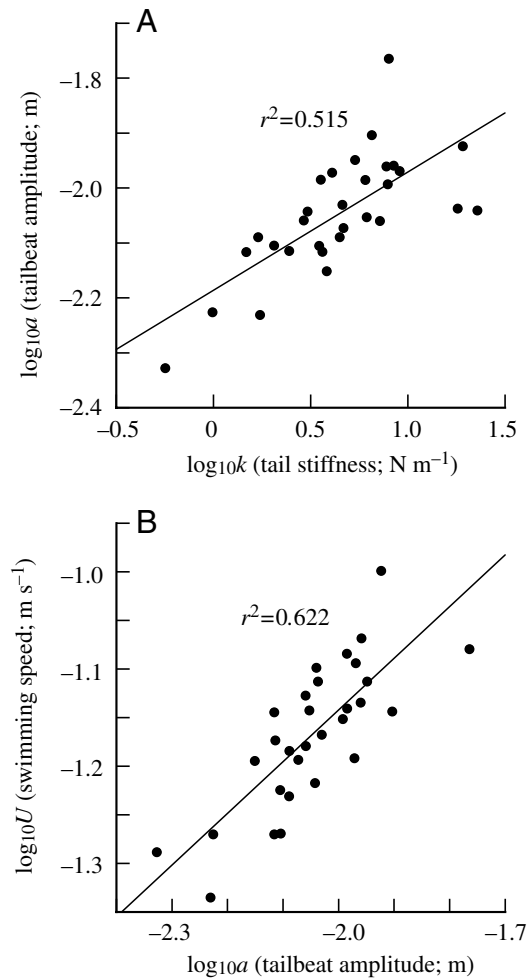


Fig. 9. Causal connection between tail stiffness k and swimming speed U . (A) Tail stiffness increases tailbeat amplitude a . (B) In turn, tailbeat amplitude increases swimming speed U . Data for biomechanical analysis are means of three straight-swimming trials for each of 30 tails. Lines indicate significant ($\alpha < 0.01$) regressions on log-transformed data.

randomly, by mutation and drift, and judged explicitly by artificial selection for adaptive value. Even in this case, using simple robots, genetics and ecology, adaptive value can be predicted only when the functional linkage between biomechanics and behavior is assessed in a specific selection environment (Brandon, 1990). When we selected for improved navigational prowess, NP , stiffness of the axial skeleton, k , determined by the biomimetic notochord's genetically based traits bending modulus, E and length, L (Eqn 1), increased as an adaptive response. However, k was neither the only trait that determined NP nor did it always evolve in synchrony with NP . Thus, even though k has both a mechanical and adaptive relation to NP , selection for NP did not in all cases evolve k . Below we discuss the complexities of this asymmetric relation by examining first mechanical and then adaptive function of the axial skeleton of biomimetic robots during forage navigation.

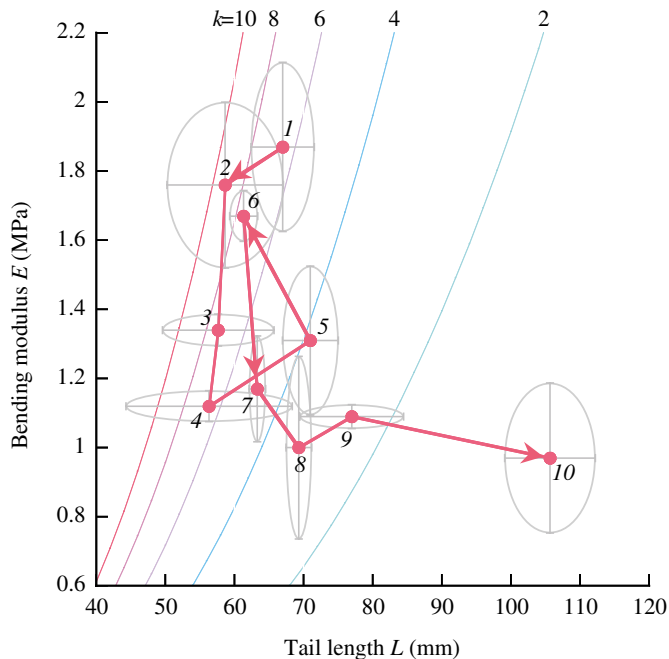


Fig. 10. Evolutionary steps in $[E, L]$ morphospace. Trajectory of the population mean from generation 1 to 10 (italic numbers). Arrowheads indicate transitions where selection was present; all transitions include change by chance (drift + mutation). The ellipses represent the population's footprint in morphospace (axes ± 1 s.e.m.). Contours represent isoclines for tail stiffness k . Note that selection operates in directions that both increase and decrease k .

A biomechanical approach: mechanical function

In terms of mechanical function, our results support Blight's hybrid-oscillator theory (Blight, 1977): stiffness of body and tail was the key parameter in controlling thrust production and, hence, swimming speed, U . When we swam our tadpole robots, 'Tadros', with a constant tailbeat frequency in a straight line, k predicted 74% of the variation in U . The causal connection between k and U was explained by only one other of the five kinematic variables measured (Table 3), lateral tailbeat amplitude, a (Fig. 9). Hence k in this system modulated thrust by increasing a .

This is not, however, the first study to demonstrate a causal relation between k , kinematics and U . Inspired by the 'half-myotome' preparation (Johnsrude and Webb, 1981), Long, Jr et al. (Long, Jr et al., 1994) swam whole-body preparations of pumpkinseed sunfish at constant tailbeat frequency, f , finding that reduced k also reduced a and U . McHenry et al. (McHenry et al., 1995) swam flexible casts of pumpkinseed sunfish, demonstrating that increased k increased the speed of the body's flexural wave of bending. In live longnose gar, reductions of the body's k reduced the f at which animals chose to swim (Long, Jr et al., 1996).

These results speak to the evolution of vertebrates insofar as they demonstrate that increases in the k of the axial skeleton (this study) and the body increase thrust production and hence U . Given that the classical adaptation hypothesis links the

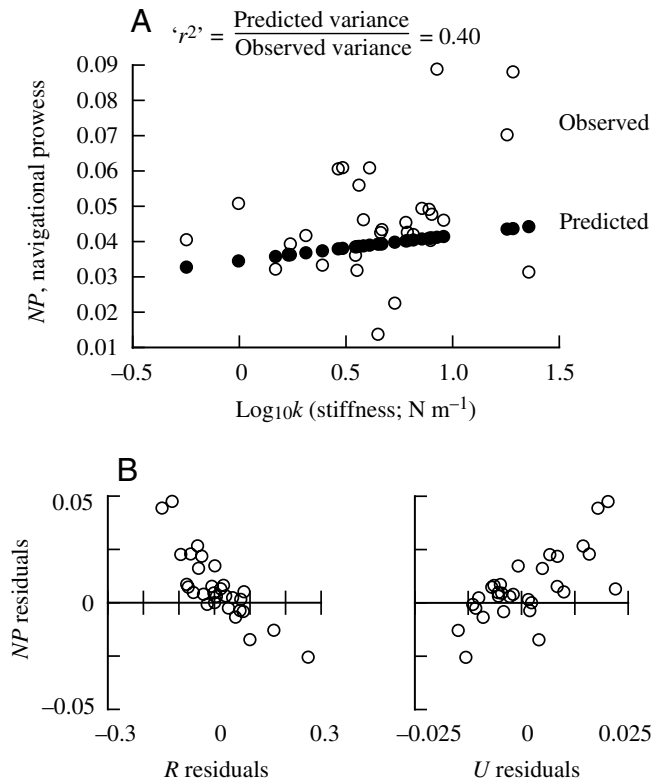


Fig. 11. Predicting navigational prowess, NP . (A) Tail stiffness k predicts NP . Predicted values of NP were generated from values of kinematic variables R , t , U and W predicted by k in univariate regressions (Table 4). Stiffness predicts 40% of the variance in NP . (B) Stiffness-independent correlates of NP . Residuals (observed minus predicted value) of NP , by definition independent of k , are correlated with the residuals of two of the four kinematic variables, orbital radius R ($P < 0.0001$) and swimming speed U ($P < 0.001$) as determined by stepwise linear regression ($r^2 = 0.81$). Residuals for kinematic variables from regression onto k . All observed values are means of 12 trials for each of three tails for ten generations ($N = 30$).

evolution of vertebrae with increased k (Webb, 1982; Weihs and Webb, 1983), we also need to know if and how vertebrae control k of the body. In preliminary experiments, in which we placed artificial vertebral ring centra onto the excised notochord of Atlantic hagfish, the presence of vertebral centra dramatically increased k of the axial skeleton by reducing the amount of connective tissue available to undergo strain during bending (Long, Jr et al., 2004a). This result is consistent with correlations between number of vertebrae and minimal propulsive wavelength during steady swimming (Long, Jr and Nipper, 1996) and body curvature during fast starts (Brainerd and Patek, 1998).

One remaining question for the biomechanist is how much of the body's k is provided by the axial skeleton? The axial skeleton provides 75% of the body's passive (without muscle contraction) flexural stiffness in hagfish and 25% in sunfish (Summers and Long, Jr, 2006). Those percentages may fall if we consider situations in which the muscle might be used to

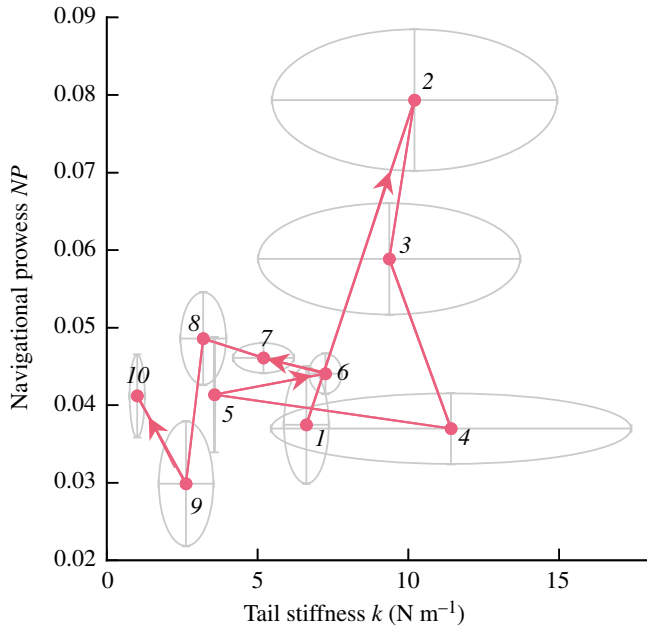


Fig. 12. Navigational and mechanical behaviors decoupled. Evolutionary trajectory of the population mean in $[NP, k]$ behavior space, from generation 1 to 10 (italic numbers). Arrowheads indicate the presence of selection. Note that while selection always acts to increase NP , two selection events increase and two decrease k . Moreover, large changes in NP , from generation 2 to 4, driven by chance, occur with little or no change in k . The points are the mean values for the population ($N=3$), and the ellipses represent the population's footprint in behavior space (axes ± 1 s.e.m.).

actively increase the body's flexural stiffness (Long, Jr and Nipper, 1996; Long, Jr, 1998).

From biomechanics alone, we see evidence to support the classical hypothesis that vertebrae stiffen the body and that increased body k increases thrust production and steady swimming speed. This formulation, however, avoids a central evolutionary question: under what ecological and selective conditions might vertebrae evolve? Unlikely is a simple relation between mechanical function (k controlling U) and adaptive function (increased U improves every behavior), given the complexities and interactions of fundamental behaviors such as navigation (Dittman and Quinn, 1996), predator evasion (Walker et al., 2005), feeding (Rice and Westneat, 2005) and foraging (Martini et al., 1997).

An evolutionary approach: adaptive function

We examined the adaptive value of k in a selection environment in which robots were rewarded for improvement in forage navigation relative to other individuals in the same population. Our fitness function (Eqn 4) gave equal weight to the four variables: orbital radius R , time to target t , U and robot wobble W , which determine the performance metric, NP (Eqn 3). Because of the biomechanical connection between k and U (see above), we designed NP to trade-off U against other important aspects of foraging, R , t and W , for which we had no *a priori* knowledge of how they related to k . We sought to create a selective environment that allowed for the emergence of different and equally successful behavioral strategies. On one end of the spectrum, a 'maneuver specialist' may evolve if the product of R , t and W decreased while U held constant; selection would act on the kinematic phenotypes related to maneuvering alone. On the other end of the spectrum, a 'speed specialist' may evolve if U increased while the product of R , t and W remained constant; selection would act on the speed phenotype alone.

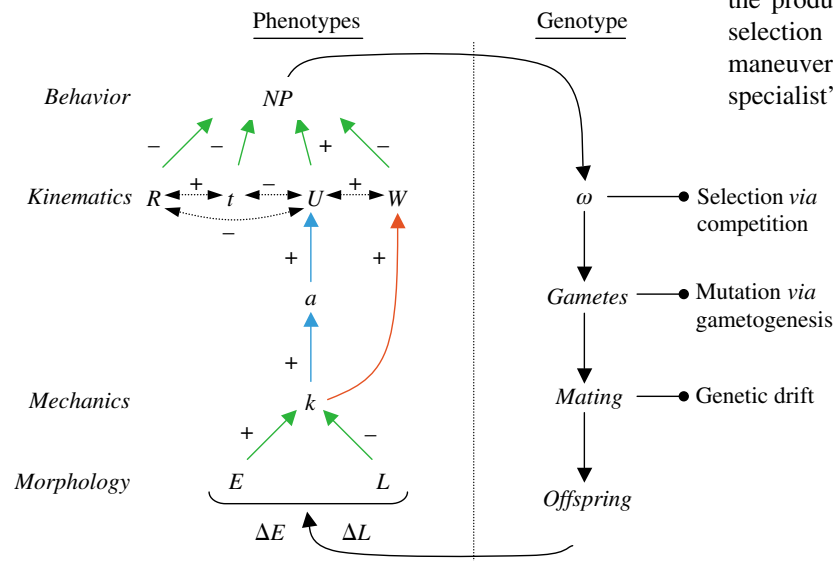


Fig. 13. Summary of the evolution of Tadros' morphology, mechanics and behavior. Plus and minus signs represent a statistically significant ($P<0.05$) correlation or regression. Blue arrows indicate relations established in biomechanical analysis (Fig. 9). Red arrow indicates relation detected only in competition trials (Fig. 8). Green arrows indicate relations by formulaic definition (Eqn 1, Eqn 3). Broken lines with double-headed arrows indicate correlations among kinematic phenotypes during competition (Table 4). Solid black lines with single-headed arrows show conceptual path of the phenotypic system through the genotypic manipulations that produce novel offspring from the adult population.

While specialist or generalist behavioral strategies might be rewarded by selection, depending on available phenotypic variance, evolution requires that selected phenotypes are heritable. In this system, therefore, the only behavioral strategies that may evolve are those linked to k , E and/or L . We found evidence for heritability of the four kinematic phenotypes that determine NP : R , t , U and W (Eqn 3). Both U and W are directly correlated with k (Fig. 8), while R and t are indirectly correlated with k through their correlation with U (Table 4; for summary, see Fig. 13).

From a 'top-down' view starting with behavior, selection for increased NP evolved a single generalist behavior in which U and W increased while R and t decreased (Figs 6, 7). It is interesting to note that NP increases in spite of the fact that increasing W removes a portion of the gains afforded by the productive changes in U , R and t . This maladaptive effect of W , seen

in the positive correlation between U and W seen during the competition experiments (Table 4), arises from maneuvering, since W was unrelated to k during the propulsion-only biomechanical tests (Fig. 8). While we did not test directly for the mechanical relation between U and W during competition, we suspect that turning maneuvers were exaggerated when the robot was swimming at higher U because the propulsive tail was also functioning as the turning rudder.

From a 'bottom-up' view starting with k , the single generalist strategy just described emerges from the summation over generational time of two different behaviors, a ' k -direct' and a ' k -indirect' mode. Recall that over all four bouts of selection, k is statistically invariant while NP increases (Fig. 7). A step-by-step view reveals that k does change under selection, two times increasing and two times decreasing while NP increases each time (Fig. 12). One explanation is that the relation between k and NP alternated between a k -direct (k increasing) and a k -indirect (k decreasing) mode. Evidence for the k -direct mode comes from NP values generated using k to predict R , t , U and W via regressions (Fig. 11A). In this k -direct mode, k predicts 40% of the variance in NP and operates directly through unequal, countervailing changes in U and W (Table 4; Fig. 8). Evidence for the k -indirect mode comes from the remaining 60% of the variance in NP unexplained by k (Fig. 11). When this variance was measured as the NP residuals, it was significantly correlated with the residuals of R and U regressed onto k (Fig. 11B). Hence R and U are the causal variables in the k -indirect mode, working together, by virtue of their inverse and direct proportionality to NP , respectively (Fig. 11B), to increase NP .

Vertebrae and vertebrae

Regarding the origin of vertebrae, as represented here by k , we examined only one of many plausible adaptation scenarios. We found evidence that vertebrae may function as an adaptation for improved navigational prowess, NP , with the stiffness they give to the axial skeleton increasing U and W directly or R and U indirectly (see previous section). While U figures in both adaptation scenarios, it is inaccurate to say that vertebrae are an adaptation for increased U . By focusing on a single aspect of behavior, like U , we miss the point that adaptation always occurs in a particular environment where selection acts upon behavior directly, with the result that many aspects of that behavior (such as R , t , U and W in this case) evolve simultaneously in integrated, independent and/or maladaptive ways.

The search for plausible adaptation scenarios for vertebrae is limited only by the imagination and resources of the investigator. We recognize that many plausible scenarios exist, and that they await testing. For example, adaptation for predation is suggested by phylogenetic reconstruction of extant taxa correlating the origin of jaws and vertebral centra (Koob and Long, Jr, 2000). Adaptation for benthic, low-speed or fin-based life histories are suggested by the phylogenetic distribution of the adult notochord, with this ancestral state

retained or secondarily reacquired in taxa such as jawless hagfish, six-gilled sharks, sturgeon, lungfish and coelocanths (Janvier, 1996). Even in closely related fish taxa, possible adaptation scenarios are numerous, with fish size, life history, acceleration and environment all correlated with changes in number of vertebrae within a family (Brainerd and Patek, 1998; McDowall, 2003). The same can be said of divergent taxa (Long, Jr and Nipper, 1996), and even the terrestrial undulatory locomotors, snakes (for a review, see Shine, 2000). Finally, selection for and pleiotropy among immune, reproductive and nervous systems may create regulatory gene networks that influence the number and morphology of vertebrae (Anand et al., 2003; Galis, 1999; Narita and Kuratani, 2005).

Caveats

When attempting to reconstruct the locomotor dynamics of fossil species, the multitude of unknown parameter values guarantees a wide range of plausible results (Hutchinson and Gatesy, 2006). Add to this the uncertainty introduced by simplifications required to model the complex interactions of genetics, phenotypes, and selection related to swimming in living vertebrates (Aubret et al., 2005; Blake, 2004; Ghalambor et al., 2003; Walker et al., 2005). At best, then, attempts to determine the adaptive value of any trait in extinct taxa can yield only what have been called 'how-possibly' adaptation explanations (Brandon, 1990). While poor resolution blurs its hindsight, BEA's simulated evolution, driven by selection and chance, offers the opportunity for unexpected results that force consideration and ranking of viable, alternative pathways.

For some, a more primary concern is the use of robots as model simulations of biology (see Webb, 2001 and the multiple critiques appended thereto). In our case, it is easy to show how the Tadros, their biomimetic tails, and the selection environment are unrealistic: in broad strokes, the individuals, their genetics, and their environment are too simple and too invariant. We have grossly oversimplified anything close to actual fish body design (Blake, 2004; Gemballa and Roder, 2004), we ignore the possibility that burst speed and tail length are related (Aubret et al., 2005), we fail to consider alternative adaptation explanations related to acceleration performance or unrelated to swimming mechanics, and we isolate locomotor systems at the cost of losing important interactions between swimming and prey capture (Rice and Westneat, 2005). The list goes on. In our defense, any modeler, whether their canvas is software or hardware, must decide what to include and what to omit. Our premise was akin to that used to justify parsimony: in the absence of a reason to include one feature over another, start with the simplest possible model that produces the desired behavior, in this case, autonomous navigation during swimming. This start-simple approach can also be supported phenomenologically, since even a single addition to a simple autonomous agent creates novel navigation behavior that is difficult to understand analytically (Braitenberg, 1984).

List of symbols and abbreviations

2D CHK	two-dimensional, cycloptic helical klinotaxis
a	lateral tail amplitude (m)
BEA	biomimetic evolutionary analysis
E	bending modulus (Pa)
f	tailbeat frequency (Hz)
I	second moment of area (m^4)
k	spring stiffness ($N\ m^{-1}$)
L	length of tail or beam (m)
N	number of gametes
NP	navigational prowess
p	genotype frequency
QTL	quantitative trait loci
R	orbital radius (m)
t	time to target (s)
U	swimming speed ($m\ s^{-1}$)
W	wobble of Tadpo (rad s^{-2})
δ	phase lateral tail displacement (% tailbeat cycle)
ϕ	tail flexion (rad)
η	Froude efficiency
ω	relative individual fitness
$\bar{\omega}$	mean fitness

Special thanks go to Janese Trimaldi, who spent many days optimizing the hydrogel fabrication process. Matthew McHenry, Hugh Crenshaw and Charles Pell graciously shared their ideas about helical klinotaxis and its robotic implementation. Robot design and fabrication was made possible by Ken Livingston, Carl Bertsche, John Vanderlee, Betsy Ketcham and Jerry Calvin. Assistance in conducting and analyzing experiments was provided by Kurt Bantilan, Nicole Doorly, Yusuke Kumai, Chun Wai Liew, Gianna McArthur, Meghan Overgaard, Robert Root and Mike Zubrow. This work was funded by National Science Foundation grants DBI-0442269 and BCS-0320764.

References

- Adams, S. R., Parsons, G. R., Hoover, J. J. and Killgore, K. J. (1997). Observations of swimming ability in shovelnose sturgeon (*Scaphirhynchus platorynchus*). *J. Freshwater Ecol.* **12**, 631-633.
- Alexander, R. McN. (2003). Achievements and limitations in the mechanics of extinct animals. In *Vertebrate Biomechanics and Evolution* (ed. V. L. Bels, J.-P. Gasc and A. Casinos), pp. 11-22. Oxford: BIOS Scientific Publishers.
- Amundson, R. and Lauder, G. V. (1994). Function without purpose: the uses of causal role function in evolutionary biology. *Biol. Philos.* **9**, 443-469.
- Anand, S., Wang, W. C. H., Powell, D. R., Bolanowski, S. A., Zhang, J., Ledje, C., Pawashe, A. B., Amemiya, C. T. and Shashikant, C. S. (2003). Divergence of Hoxc8 early enhancer parallels diverged axial morphologies between mammals and fishes. *Proc. Natl. Acad. Sci. USA* **100**, 15666-15669.
- Arnold, S. J. (2003). Performance surfaces and adaptive landscapes. *Integr. Comp. Biol.* **43**, 367-375.
- Aubret, F., Bonnet, X. and Maumelat, S. (2005). Tail loss, body condition, and swimming performances in tiger snakes, *Notechis ater* Occidentalis. *J. Exp. Zool. Part A Comp. Exp. Biol.* **303**, 894-903.
- Bels, V. L., Gasc, J.-P. and Casinos, A. (ed.) (2003). *Vertebrate Biomechanics and Evolution*. Oxford: BIOS Scientific Publishers.
- Benhamou, S. (2004). How to reliably estimate the tortuosity of an animal's path: straightness, sinuosity, or fractal dimension? *J. Theor. Biol.* **229**, 209-220.
- Blake, R. W. (2004). Fish functional design and swimming performance. *J. Fish Biol.* **65**, 1193-1222.
- Blight, A. R. (1977). Muscular control of vertebrate swimming movements. *Biol. Rev.* **52**, 181-218.
- Brainerd, E. L. and Patek, S. N. (1998). Vertebral column morphology, C-start curvature, and the evolution of mechanical defenses in tetraodontiform fishes. *Copeia* **4**, 971-984.
- Braitenberg, V. (1984). *Vehicles: Experiments in Synthetic Psychology*. Cambridge, MA: MIT Press.
- Brandon, R. N. (1990). *Adaptation and Environment*. Princeton, NJ: Princeton University Press.
- Delsuc, F., Brinkmann, H., Chourrout, D. and Phillippe, H. (2006). Tunicates and not cephalochordates are the closest living relatives of vertebrates. *Nature* **439**, 965-968.
- Dittman, A. H. and Quinn, T. P. (1996). Homing in Pacific salmon: mechanisms and ecological basis. *J. Exp. Biol.* **199**, 83-91.
- Galis, F. (1999). On the homology of structures and Hox genes: the vertebral column. *Novartis Found. Symp.* **222**, 80-91.
- Gardiner, B. (1983). Gnathostome vertebrae and the classification of the amphibia. *Zool. J. Linn. Soc.* **79**, 1-59.
- Garland, T., Jr (2003). Selection experiments: an under-utilized tool in biomechanics and organismal biology. In *Vertebrate Biomechanics and Evolution* (ed. V. L. Bels, J.-P. Gasc and A. Casinos), pp. 23-56. Oxford: BIOS Scientific Publishers.
- Gemballa, S. and Roder, K. (2004). From head to tail: the myoseptal system in basal actinopterygians. *J. Morphol.* **259**, 155-171.
- Ghalambor, C. K., Walker, J. A. and Reznick, D. N. (2003). Multi-trait selection, adaptation, and constraints on the evolution of burst swimming performance. *Integr. Comp. Biol.* **43**, 431-438.
- Gillespie, J. H. (2004). *Population Genetics: A Concise Guide* (2nd edn). Baltimore, MD: The Johns Hopkins University Press.
- Goodrich, E. S. (1930). *Studies on the Structure and Development of Vertebrates*. London: Macmillan.
- Hutchinson, J. R. and Gatesy, S. M. (2006). Dinosaur locomotion: beyond the bones. *Nature* **440**, 292-294.
- Janvier, P. (1996). *Early Vertebrates*. Oxford: Clarendon.
- Johnsrude, C. I. and Webb, P. W. (1985). Mechanical properties of the myotomal musculo-skeletal system of rainbow trout, *Salmo gairdneri*. *J. Exp. Biol.* **119**, 171-177.
- Kingsolver, J. G. and Koehl, M. A. R. (1985). Aerodynamics, thermoregulation, and the evolution of insect wings: differential scaling and evolutionary change. *Evolution* **39**, 488-504.
- Koob, T. J. and Hernandez, D. J. (2003). Mechanical and thermal properties of novel polymerized NDGA-gelatin hydrogels. *Biomaterials* **24**, 1285-1292.
- Koob, T. J. and Long, J. H., Jr (2000). The vertebrate body axis: evolution and mechanical function. *Am. Zool.* **40**, 1-18.
- Laerm, J. (1976). The development, function, and design of amphicoelous vertebrae in teleost fish. *Zool. J. Linn. Soc.* **58**, 237-254.
- Laerm, J. (1979). The origin and homology of the chondrosteal vertebral centrum. *Can. J. Zool.* **57**, 475-485.
- Lauder, G. V. (1980). On the relationship of the myotome to the axial skeleton in vertebrate evolution. *Paleobiology* **6**, 51-56.
- Lauder, G. V. (1995). On the inference of function from structure. In *Functional Morphology in Vertebrate Paleontology* (ed. J. J. Thomason), pp. 1-18. Cambridge: Cambridge University Press.
- Long, J. H., Jr (1995). Morphology, mechanics, and locomotion: the relation between the notochord and swimming motions in sturgeon. *Environ. Biol. Fishes* **44**, 199-211.
- Long, J. H., Jr (1998). Muscles, elastic energy, and the dynamics of body stiffness in swimming eels. *Am. Zool.* **38**, 771-792.
- Long, J. H., Jr and Nipper, K. S. (1996). The importance of body stiffness in undulatory propulsion. *Am. Zool.* **36**, 678-694.
- Long, J. H., Jr, McHenry, M. J. and Boetticher, N. C. (1994). Undulatory swimming: how traveling waves are produced and modulated in sunfish (*Lepomis gibbosus*). *J. Exp. Biol.* **192**, 129-145.
- Long, J. H., Jr, Hale, M. E., McHenry, M. J. and Westneat, M. W. (1996). Functions of fish skin: flexural stiffness and steady swimming of longnose gar, *Lepisosteus osseus*. *J. Exp. Biol.* **199**, 2139-2151.
- Long, J. H., Jr, Koob-Emunds, M., Sinwell, B. and Koob, T. J. (2002). The notochord of hagfish, *Myxine glutinosa*: viscoelastic properties and mechanical functions during steady swimming. *J. Exp. Biol.* **205**, 3819-3831.
- Long, J. H., Jr, Lammert, A. C., Strother, J. and McHenry, M. J. (2003). Biologically-inspired control of perception-action systems: helical klinotaxis

- in 2D robots. In *Proceedings of the 13th International Symposium on Unmanned Untethered Submersible Technology (UUST)*. Lee, NH: Autonomous Undersea Systems Institute.
- Long, J. H., Jr, Koob-Emunds, M. and Koob, T. J.** (2004a). The mechanical consequences of vertebral centra. *Bull. Mt. Desert Isl. Biol. Lab. Salish. Cove Maine* **43**, 99-101.
- Long, J. H., Jr, Lammert, A. C., Pell, C. A., Kemp, M., Strother, J., Crenshaw, H. C. and McHenry, M. J.** (2004b). A navigational primitive: biorobotic implementation of cycloptic helical klinotaxis in planar motion. *IEEE J. Oceanic Eng.* **29**, 795-806.
- Long, J. H., Jr, Engel, V., Combie, K., Koob-Emunds, M. and Koob, T. J.** (2006a). A target for biomimetics and synthetic biology: the notochord of the Atlantic hagfish, *Myxine glutinosa*. *Bull. Mt. Desert Isl. Biol. Lab. Salish. Cove Maine* **45**, 78-81.
- Long, J. H., Jr, Schumacher, J., Livingston, N. and Kemp, M.** (2006b). Four flippers or two? Tetrapodal swimming with an aquatic robot. *Bioinsp. Biomim.* **1**, 20-29.
- Martini, F. H., Lesser, M. P. and Heiser, J. B.** (1997). Ecology of the hagfish, *Myxine glutinosa* L. in the Gulf of Maine. II. Potential impact on benthic communities and commercial fisheries. *J. Exp. Mar. Biol. Ecol.* **214**, 97-106.
- McDowall, R. M.** (2003). Variation in vertebral number in galaxiid fishes (Teleostei: Galaxiidae): a legacy of life history, latitude and length. *Environ. Biol. Fishes* **66**, 361-381.
- McHenry, M. J. and Strother, J. A.** (2003). The kinematics of phototaxis in larvae of the ascidian *Aplidium constellatum*. *Mar. Biol.* **142**, 173-184.
- McHenry, M. J., Pell, C. A. and Long, J. H., Jr** (1995). Mechanical control of swimming speed: stiffness and axial wave form in an undulatory fish model. *J. Exp. Biol.* **198**, 2293-2305.
- Narita, Y. and Kuratani, S.** (2005). Evolution of the vertebral formulae in mammals: a perspective on developmental constraints. *J. Exp. Zool. B Mol. Dev. Evol.* **304**, 91-106.
- Nolfi, S. and Floreano, D.** (2000). *Evolutionary Robotics: The Biology, Intelligence, and Technology of Self-Organizing Machines*. Cambridge, MA: MIT Press.
- Pabst, D. A.** (1996). Springs in swimming animals. *Am. Zool.* **36**, 723-735.
- Rice, A. N. and Westneat, M. W.** (2005). Coordination of feeding, locomotor and visual systems in parrotfishes (Teleostei: Labridae). *J. Exp. Biol.* **208**, 3503-3518.
- Ridley, M.** (1993). *Evolution*. Cambridge, MA, USA: Blackwell Scientific.
- Rockwell, H., Evans, F. G. and Pheasant, H. C.** (1938). The comparative morphology of the vertebrate spinal column: its form as related to function. *J. Morphol.* **63**, 87-117.
- Shine, R.** (2000). Vertebral numbers in male and female snakes: the roles of natural, sexual and fecundity selection. *J. Evol. Biol.* **13**, 455-465.
- Sulak, K. J., Edwards, R. E., Hill, G. W. and Randall, M. T.** (2002). Why do sturgeons jump? Insights from acoustic investigations of the Gulf sturgeon in the Suwannee River, Florida, USA. *J. Appl. Ichthyol.* **18**, 617-620.
- Summers, A. P. and Long, J. H., Jr** (2006). Skin and bones, sinew and gristle: the mechanical behavior of fish skeletal tissues. In *Fish Physiology: Fish Biomechanics*. Vol. 23 (ed. R. E. Shadwick and G. V. Lauder), pp. 141-177. New York: Academic Press.
- Terada, Y. and Yamamoto, I.** (2004). An animatronic system including lifelike robotic fish. *Proc. IEEE* **92**, 1814-1820.
- Travisano, M., Mongold, J. A., Bennett, A. F. and Lenski, R. E.** (1995). Experimental tests of the roles of adaptation, chance, and history in evolution. *Science* **267**, 87-90.
- Triantafyllou, G. S., Triantafyllou, M. S. and Grosenbaugh, M. A.** (1993). Optimal thrust development in oscillating foils with application to fish propulsion. *J. Fluids Struct.* **7**, 205-224.
- Walker, J. A., Ghalambor, C. K., Griset, O. L., McKenney, D. and Reznick, D. N.** (2005). Do faster starts increase the probability of evading predators? *Funct. Ecol.* **19**, 808-815.
- Webb, B.** (2001). Can robots make good models of biological behavior? *Behav. Brain Sci.* **24**, 1033-1050.
- Webb, P. W.** (1982). Locomotor patterns in the evolution of actinopterygian fishes. *Am. Zool.* **22**, 329-342.
- Weihs, D. and Webb, P. W. (ed.)** (1983). Optimization of locomotion. In *Fish Biomechanics*, pp. 339-371. New York: Praeger.
- Zar, J. H.** (1996). *Biostatistical Analysis* (3rd edn). Upper Saddle River, NJ: Prentice-Hall.